Charge transport mechanisms in monovalent doped mixed valent manganites

Hetal Boricha[1], Zalak Joshi[1], Davit Dhruv[1], K.N. Rathod[1], Keval Gadani[1], D.D. Pandya[1], Sanjay Kansara[1], C.M. Thaker[2], S. Rayaprol[3], P.S. Solanki[1], N.A. Shah[1*]

[1]*Department of Physics, Saurashtra University, Rajkot, 360005, India*
[2]*M.V.M. Science and Home Science College, Rajkot, 360005, India*
[3]*UGC-DAE Consortium for Scientific Research, Mumbai Center, B.A.R.C. Campus, Mumbai, 400 085, India*

[*]Corresponding author, E-mail: snikesh@yahoo.com; Tel: (+91) 2812588428

Received: 30 March 2016, Revised: 02 August 2016 and Accepted: 03 August 2016

DOI: 10.5185/amp.2016/117
www.vbripress.com/amp

Abstract

In this communication, we report the results of the studies on structural and transport properties of monovalent Na^+ doped $La_{1-x}Na_xMnO_3$ (LNMO; x = 0.00, 0.05, 0.10, 0.15, 0.20, 0.25 and 0.30) manganites synthesized by conventional ceramic method. X-ray diffraction (XRD) and Rietveld refinements reveal the single phasic nature of LNMO manganites without any detectable impurity within the measurement range. Temperature dependent resistivity, under different applied magnetic fields, has been performed on LNMO samples. Samples understudy exhibit metal to insulator (semiconductor) transition at temperature T_P which is strongly influenced by the substitution of Na^+ at La^{3+} site. ρ – T plots also exhibit resistivity upturn behavior at low temperature well below 40K under all the applied fields. Variation in T_P and resistivity has been discussed in the context of the competition between the transport favoring tolerance factor and zener double exchange (ZDE) mechanism and transport degrading Jahn–Teller (JT) and size variance effects. In order to understand the mechanisms responsible for the charge transport in metallic and semiconducting regions and to explore the possible electronic processes responsible for the observed low temperature resistivity minima in all the presently studied LNMO manganites, various models have been employed. It has been found that VRH mechanism gets successfully fitted to the resistivity data in the semiconducting region while ZDE polynomial law is responsible for the charge conduction in metallic region for all the presently studied LNMO samples. A strong dependence of activation energy on the Na^+ – content as well as applied magnetic field has been discussed in the context of variation and interrelations between the structural parameters. Charge conduction in metallic region has been discussed in the light of electron–phonon interactions which is influenced by the Na^+ – content and applied magnetic field. Electrostatic blockade model has been employed to understand the low temperature resistivity minima behavior. Blocking energy for the charge carriers shows a dependence on the magnetic energy provided to the charge carriers. Present study can be useful to understand and to control the charge conduction in the manganites and hence to design the manganite based thin film devices for various spintronic applications.

Keywords: Manganite, ceramic method, monovalent, charge transport, transport properties.

Introduction

Mixed valent manganites having the general formula $La_{1-x}A_xMnO_3$ (A is the monovalent, divalent or tetravalent ions) exhibit interesting and interrelated fascinating properties mainly due to their highly correlated electrons **[1]**. Manganites are mainly known for metal to insulator transition at temperature T_P and ferromagnetic to paramagnetic transition at temperature T_C, exhibit by them. These properties are highly affected by different structural parameters such as average ionic radius, size variance, carrier density and tolerance factor **[2, 3]**. Manganites are also known for magnetoresistance (MR) effect exhibited by them. MR can be tuned at low temperature under either low applied magnetic field **[4, 5]** or high applied magnetic field **[4, 5]** (known as extrinsic components of MR) else at high temperature near about transition temperatures **[6, 7]** (known as intrinsic MR). Origin of MR and conduction of charge carriers (i.e. electrons) can be explained on the basis of zener double exchange (ZDE) mechanism **[8, 9]**. Later on, it was realized that ZDE mechanism cannot alone explain the charge transport mechanisms in mixed valent manganites **[10]**. Hence, Jahn–Teller (JT) distortion was used to understand the role of disorder in the magnetic lattice of manganites. In addition to ZDE mechanism and JT distortion, few other phenomena such as electron–electron scattering, electron–phonon coupling, lattice polaron, lattice magnon, charge ordering, orbital

ordering, spin ordering, phase separation, phase coexistence, phase segregation, etc have also been introduced to make clear the physics of electronic charge transport across the manganite lattice.

All these above mentioned aspects of manganites and their charge transport mechanisms are strongly influenced by sintering temperature **[4]**, applied magnetic field **[11, 12]**, applied electric field **[13]**, film thickness **[6]**, temperature **[14]**, synthesis technique **[15]**, charge carrier density **[15]**, substitutional effects at A–site **[15]** and B–site **[10, 16]**, etc. Solanki *et al***. [4]** have studied the effect of sintering temperature on the charge transport mechanism responsible for the low temperature resistivity anomaly in the context of electron–electron scattering process. Doshi *et al* **[11]** have studied the effect of applied magnetic field on the activation energy of charge carriers in semiconducting region of high resistive doped charge ordered mixed valent manganites using variable range hopping mechanism. Very recent, Krichene *et al* **[12]** have reported the percolation studies under a large temperature range for magnetic field dependent resistivity–temperature data [ρ–T (H)] obtained for $La_{0.5}Ca_{0.5}Mn_{0.998}Bi_{0.02}O_3$ charge ordered manganite. Solanki *et al* **[13]** have investigated the effect of applied electric field on the charge transport mechanism across the ZnO / manganite and manganite / conducting substrate interfaces using thermionic emission mechanism at room temperature. Effect of film thickness on the low temperature electron–electron scattering for manganite films has been reported using a strong disorder induced coulombic interactions between the charge carriers and its dependence on film thickness **[6]**. Temperature dependent current–voltage characteristics and related charge transport processes across the manganite based interfaces have been discussed in the context of thermionic emission mechanism for manganite based heterostructure **[14]**. Recently, charge transport mechanisms for low temperature resistivity minima, metallic behavior and semiconducting behavior have been investigated for the chemically grown manganite films and its dependence upon the synthesis technique, charge carrier density and A–site substitution **[15]**. For understanding of B–site substitutional effects on the charge transport mechanisms responsible for different temperature ranges, various theoretical models have been used for $La_{0.5}Ca_{0.5}Mn_{1-x}Bi_xO_3$ charge ordered manganites **[16]**. Recently, the similar studies have been carried out for Al–substituted $La_{0.7}Ca_{0.3}Mn_{1-x}Al_xO_3$ mixed valent manganites by Rathod et al **[11]**. All these reports **[4, 6, 11 – 16]** strongly suggest that charge conduction mechanisms should be well understood to design appropriate manganite based thin film devices useful for various spintronic applications.

In fact, strong spin polarization becomes weak upon increasing the temperature as a consequence of thermal fluctuations across the spin alignment. This is one of the most critical problems of colossal magnetoresistance (CMR) manganites in their practical applications near room temperature. As a result of thermal fluctuations induced weakening of spin polarization in manganites, their intrinsic transition temperature T_C becomes higher as compared to their extrinsic transition temperature T_P, which is the most observed case in manganites **[16]**. If $T_P > T_C$, this problem can be overcome for some practical applications of manganites in realizing spintronic device operations near room temperature. Monovalent doped mixed valent manganites exhibit large T_P as compared to their T_C which can be useful for their practical potential in device applications. In addition, monovalent doped mixed valent manganites possess a strong spin polarization, high transition temperatures and appreciably large MR at low as well as high temperatures which is suitable for their potential applications **[17 – 23]**. Particularly, sodium (Na^+) doped manganites have been studied well in the form of polycrystalline bulk and nanostructure for various physical properties **[21 – 23]**. Ho et al **[21]** have studied the magnetic properties of sodium doped $La_{0.7}Ca_{0.3-x}Na_xMnO_3$ manganites wherein they have also discussed the magnetocaloric effect for these compounds. Ehi–Eromosele et al **[22]** have investigated the structural, microstructural and magnetic properties of complex $La_{1-x}Na_yMnO_3$ ($y \leq x$) nanostructured manganites grown using solution combustion method. Recently, Arunachalam et al **[23]** have performed ultrasonic studies on Na+ – doped $LaMnO_3$ manganites.

Keeping in mind all the above aspects of mixed valent manganites, their application capabilities in various potential fields, fascinating featured characteristics of monovalent doped mixed valent manganites and importance of investigations on the charge transport mechanisms in these compounds, in the present communication, we report the results of the detailed studies on the transport properties of sodium doped $La_{1-x}Na_xMnO_3$ (LNMO; x = 0.05, 0.10, 0.15, 0.20, 0.25 and 0.30) mixed valent manganites. Various models and mechanisms have been employed to understand the charge conduction in these compounds and their strong dependence on the Na^+ – content and applied magnetic field has also been discussed in detail. Results and parameters, obtained from the charge conduction mechanisms and models fitted to the resistivity data, have been discussed in the context of structural parameters, ZDE mechanism and JT effect. Present study provides a complete understanding of charge conduction mechanisms governing the resistivity behavior of monovalent sodium doped $LaMnO_3$ manganites. An attempt has been made to explore the responsible charge transport mechanisms for all the three regions, semiconducting, metallic and low temperature, in $La_{1-x}Na_xMnO_3$ manganites.

Experimental

Materials

La_2O_3: Sigma Aldrich (make); 99.99% (purity); USA (place of manufacturing). MnO_2: Sigma Aldrich (make); 99.99% (purity); USA (place of manufacturing). Na_2CO_3: Sigma Aldrich (make); 99% (purity); India (place of manufacturing)

Material synthesis

Polycrystalline samples of $La_{1-x}Na_xMnO_3$ (LNMO; x = 0.05, 0.10, 0.15, 0.20, 0.25 and 0.30) mixed valent manganites were synthesized by using conventional ceramic route. Starting materials La_2O_3 and MnO_2 were initially preheated at 550°C while Na_2CO_3 was preheated at 350°C for 4h. Dried (preheated) powders were then mixed in stoichiometric ratio and ground for a long time (more than 6h) followed by calcination at 950°C for 24h. Calcined mixtures of powders of all the samples were then again ground for 6h and then pelletized and intermediate sintered at 1050°C for 48h. Pellets were broken into powder form again ground for 6h and finally pelletized and sintered at 1150°C for 72h in air environment. Hereafter, sample having Na–content x = 0.05, 0.10, 0.15, 0.20, 0.25 and 0.30 are referred as LN05, LN10, LN15, LN20, LN25 and LN30, respectively.

Characterizations

To understand the structural purity, phase present and crystalline nature of all the samples, X-ray diffraction (XRD) was performed at room temperature using Cu Kα radiation using Philips make diffractometer (model: PW 3040/60, X'pert PRO). For structural analysis, Rietveld refinements using standard FULLPROF code **[24]** were carried out on all the XRD results of presently studied compounds. Transport properties were investigated by performing electrical resistivity and magnetoresistance measurements using standard four probe method using physical property measurement system (PPMS) in the temperature range: 5 – 300K under applied magnetic field range: 0 – 8T.

Results and discussion

Fig. 1 shows typical XRD patterns of **(a)** $La_{0.95}Na_{0.05}MnO_3$ (LN05) and **(b)** $La_{0.70}Na_{0.30}MnO_3$ (LN30) manganites revealing a single phasic nature of all the compounds understudy without any detectable impurity within the measurement range. It is clear from figure 1 that XRD peaks shift toward lower 2θ suggests an increase in lattice parameters and unit cell volume with increase in Na–content (x). All the XRD patterns of LNMO samples were refined using Rietveld refinements by employing FULLPROF code **[24]**, as shown in. All the presently studied compounds possess rhombohedral unit cell structure having R–3C space group (no. 167). Rietveld refinements confirm no structural phase transition upon substitution of Na^+ at La^{3+} site, within the substitution range studied. Small fluctuations in the difference line observed in **Fig. 1 (c)** for all the samples suggest a good agreement between the experimental and calculated values of patterns. **Table 1** lists the values of lattice parameters and cell volume for all the $La_{1-x}Na_xMnO_3$ (LNMO) compounds. Enhancement in lattice parameters and cell volume can be ascribed to the modifications in the structural features with increase in Na–content (x) which is larger ion (1.24Å) substituted at smaller ionic La–site (1.216Å). **Table 1** also lists the values of average A–site ionic radius ($\langle r_A \rangle$), A–site size variance (σ_A^2) and tolerance factor (t) for LNMO samples understudy, calculated using the reported formulae **[15, 25]**. It can be understood that with increase in larger ion Na–content (x), $\langle r_A \rangle$, σ_A^2 and t get increased **(Table 1)**.

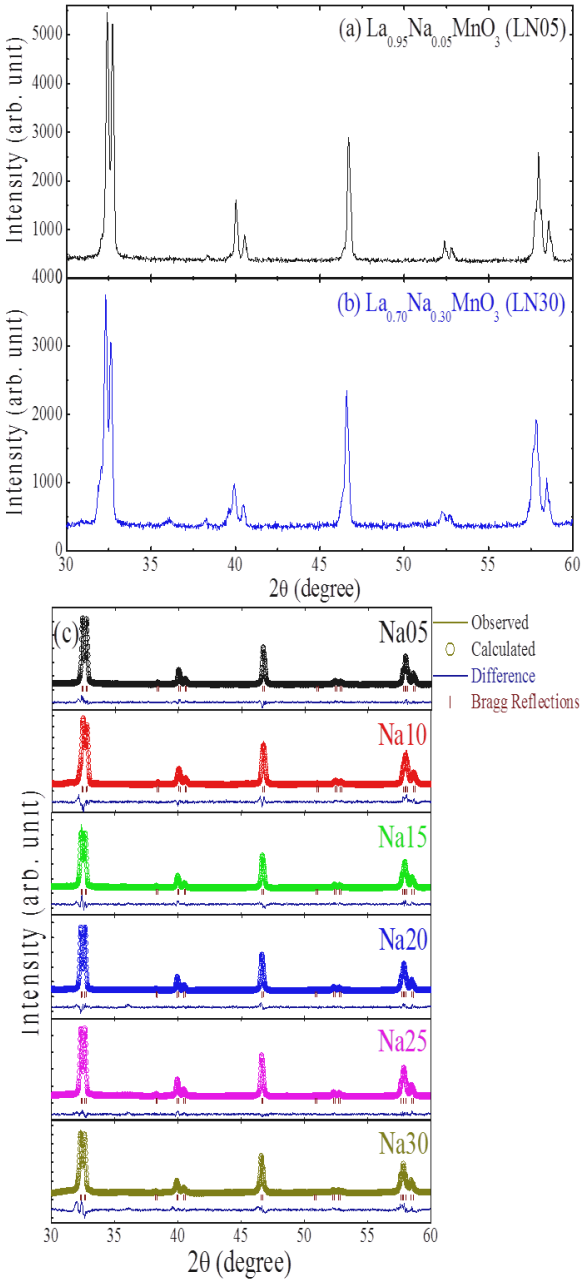

Fig. 1. Typical XRD patterns of (a) $La_{0.95}Na_{0.05}MnO_3$ (LN05; x = 0.05) and (b) $La_{0.70}Na_{0.30}MnO_3$ (LN30; x = 0.30) manganites. (c) Rietveld refined XRD patterns of $La_{1-x}Na_xMnO_3$ (LNMO; x = 0.05, 0.10, 0.15, 0.20, 0.25 and 0.30) manganites

Table 1. Values of lattice parameters, cell volume (V), average A¬–site ionic radius (<rA>), A–site size variance (σA2) and tolerance factor (t) for La1–xNaxMnO3 (LNMO; x = 0.05, 0.10, 0.15, 0.20, 0.25 and 0.30) manganites

Sample	a = b (nm)	c (nm)	V (nm^3)	$<r_A>$ (nm)	σ_A^2 (nm^2)	t
LN05	0.5525 (5)	1.3347 (1)	0.4074	0.1217	2.74E–7	0.908
LN10	0.5526 (7)	1.3349 (9)	0.4076	0.1218	5.18E–7	0.914
LN15	0.5527 (7)	1.3357 (2)	0.4080	0.1220	7.34E–7	0.919
LN20	0.5534 (5)	1.3366 (8)	0.4093	0.1221	9.22E–7	0.925
LN25	0.5535 (3)	1.3369 (6)	0.4096	0.1222	1.08E–6	0.931
LN30	0.5538 (6)	1.3371 (7)	0.4101	0.1223	1.21E–6	0.936

Fig. 2 shows the variation in resistivity with temperature under applied magnetic fields of (a) 0T, (b) 1T, (c) 5T and (d) 8T for presently studied all the LNMO samples. Under 0T applied magnetic field, all the samples show metal ($d\rho / dT > 0$) to insulator ($d\rho / dT < 0$) transition at temperature T_P. Variation in peak resistivity (ρ_P) and T_P with Na–content (x) for LNMO samples can be understood as:

(a) Observation of transition temperature T_P ~ 257K in LN05 sample: (i) $LaMnO_3$ (undoped pure sample) is JT compound having insulating electrical behavior. Substitution of larger sized Na^+ (1.24Å) ion at smaller sized La^{3+} (1.216Å) ionic site results in the enhancement in Mn–O–Mn bond angle deviated from 180°, (ii) substitution of larger sized Na^+ (1.24Å) ion at smaller sized La^{3+} (1.216Å) ionic site also results in the enhanced tolerance factor from 0.902 in $LaMnO_3$ to 0.908 in LN05, (iii) upon substitution of Na–content (x), double (2x) Mn^{4+} get generated in the lattice resulting in a strong ZDE mechanism and (iv) reduction in number of Mn^{3+} ions eliminates the possibility of related JT effect in the lattice. These reasons explain the observation of metal to insulator transition temperature in 5% Na^+ doped $LaMnO_3$ manganite (LN05).

(b) T_P increases from 257K (LN05) to 286K (LN15) while resistivity gets suppressed throughout the temperature range studied: (i) tolerance factor increases from 0.908 to 0.919 resulting in an enhanced charge carrier movement across the lattice, (ii) density of Mn^{4+} ions and hence $Mn^{3+} – O^{2–} – Mn^{4+}$ ionic pairs increase with increase in Na–content (x) from 0.05 to 0.15 resulting in a strong ZDE mechanism across the lattice and (iii) increased number of Mn^{4+} ions in the lattice and hence decreased number of Mn^{3+} ions reduces overall JT effect. These may be the causes for the suppression in resistivity and shifting of T_P towards higher temperature with increase in Na–content (x) from 0.05 to 0.15.

(c) Further increase in Na–content (x) from 0.15 to 0.30 shifts T_P towards lower temperature from 286K (LN15) to 264K (LN30) while resistivity gets enhanced: (i) in addition to the favorable conditions such as improved tolerance factor, strengthened ZDE mechanism and suppressed JT effect upon increase in Na–content (x), A–site size variance increases continuously from x = 0.05 to x = 0.30 **(Table 1)** which favors the rise in the resistivity in the samples. This entertains a strong competition between the transport favorable conditions (tolerance factor, ZDE mechanism and weakening of JT effect) and inconsistent size variance effect. For the LNMO samples having $x \leq 0.15$ possess dominance of transport favorable conditions while for $x > 0.15$ samples, size variance effect plays an important principal role in governing the transport mechanism. This is one of the most important causes for the observation of reduced T_P and enhanced resistivity in the samples with $x > 0.15$ with increase in Na–content (x), (ii) increase in Na–content (x) with $x > 0.15$, large number of available $Mn^{4+} – O^{2–} – Mn^{4+}$ ionic pairs supports the super exchange mechanism leading to increase in resistivity and decrease in TP with increase in Na–content (x) from 0.15 to 0.30.

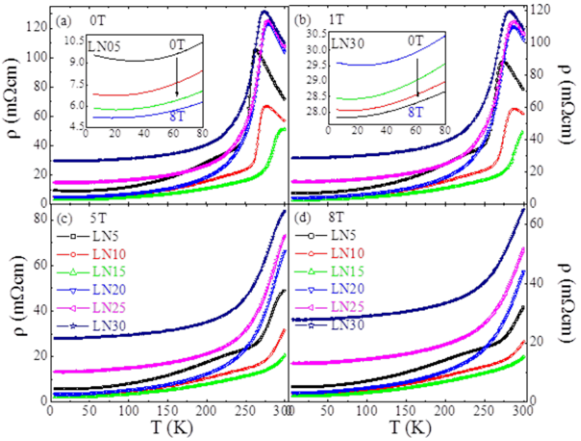

Fig. 2. Variation in resistivity with temperature under applied magnetic fields of (a) 0T, (b) 1T, (c) 5T and (d) 8T for $La_{1-x}Na_xMnO_3$ (LNMO; x = 0.05, 0.10, 0.15, 0.20, 0.25 and 0.30) manganites. Insets: Magnetic field dependent ρ – T plots of LN05 and LN30 samples understudy in the temperature range: 0 – 80K

Upon increase in applied magnetic field from 0T to 1T **[Fig. 2 (b)],** 5T **[Fig. 2 (c)]** and 8T **[Fig. 2 (d)]** overall resistivity decreases throughout the temperature range studied suggesting that all the LNMO samples understudy exhibit negative MR. As shown in **Fig. 2 (b),** under 1T applied magnetic field, variation in resistivity and T_P remains the same as shown in figure 3 (a) for 0T applied field. Further increase in applied magnetic field from 1 to 5 and 8T, all the samples show only metallic behavior in the ρ – T plots. Suppression in resistivity throughout the temperature range studied and absence of transition temperatures under 5 and 8T applied magnetic fields for all the LNMO samples can be ascribed to the magnetic field induced suppression in the scattering of the charge carriers at the grain boundaries and reduction in the magnetic disorder at Mn–O–Mn bond angles resulting in the strengthened ZDE mechanism across the magnetic lattice of LNMO manganites. Insets of **Fig. 2** show the ρ – T plots of LN05 and LN30 samples understudy in the temperature range: 0 – 40K revealing the resistivity minima behavior under all the applied magnetic fields studied which will be discussed later in this article.

In order to understand the charge transport mechanism responsible for the insulating behavior,

metallic nature and low temperature resistivity character of presently studied LNMO samples, various theoretical models and mechanisms have been employed by fitting the experimental resistivity data in different temperature regions. Under zero and 1T applied magnetic fields, all the LNMO samples (except LN15, since it shows only metallic behavior up to 300K) exhibit insulating (semiconducting) behavior which becomes metallic in nature under high applied magnetic fields of 5 and 8T.

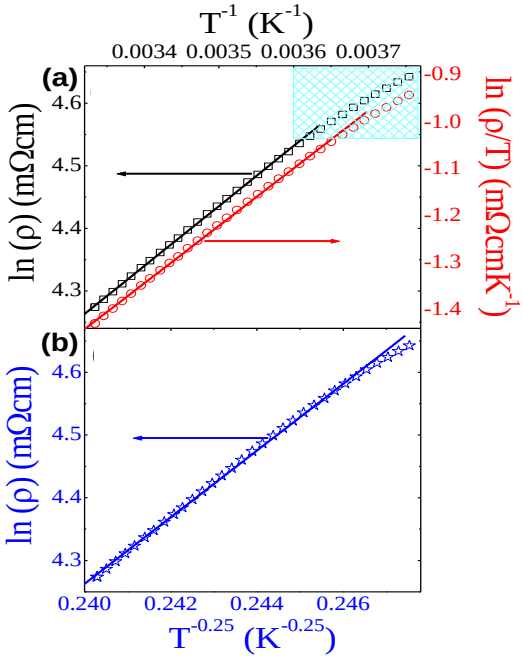

Fig. 3. Plots of fitting of resistivity data to (a) ln ρ vs. T^{-1} and ln (ρ/T) vs. T^{-1} and (b) ln ρ vs. $T^{-0.25}$ in semiconducting region under zero applied magnetic field for $La_{0.95}Na_{0.05}MnO_3$ (LN05; x = 0.05) manganite

This can be due to the fact that magnetic field can improve the charge conduction and hence shift the transition temperature towards higher temperature, well above 300K. To understand the charge transport mechanism for insulating region (well above T_P) in manganites, various theoretical mechanisms and models such as nearest neighbor hopping **[26]**, adiabatic nearest neighboring hopping model for small polaron conduction **[27]**, Shklovskii – Efros (SE) type of variable range hopping (VRH) model **[28]** and Mott type VRH model for uncorrelated carriers **[29, 30]** can be used to fit the obtained experimental resistivity data. Three of them, namely, (i) nearest neighbor hopping model [$\rho = \rho_0 \exp(E_a/KT)$], (ii) small polaron conduction [$\rho = AT \exp(E_a/KT)$] and (iii) Mott type VRH model [$\rho = \rho_0 \exp(T_O/T)^{1/4}$] were fitted to resistivity data under zero applied field for LN05 manganite sample as shown in **Fig. 3**. It is clearly seen that experimental data in semiconducting (insulating) region does not follow nearest neighboring hopping or small polaron conduction mechanism **[Fig. 3 (a)]**, particularly, near the transition temperature (T_P) (indicated by light cyan colored square box). Linearly fitted data of resistivity in the form of ln ρ vs $T^{-0.25}$ **[Fig. 3 (b)]** suggests that in semiconducting region of LN05, resistivity of LN05 sample follows Mott type VRH mechanism throughout the temperature range (well above T_P) studied.

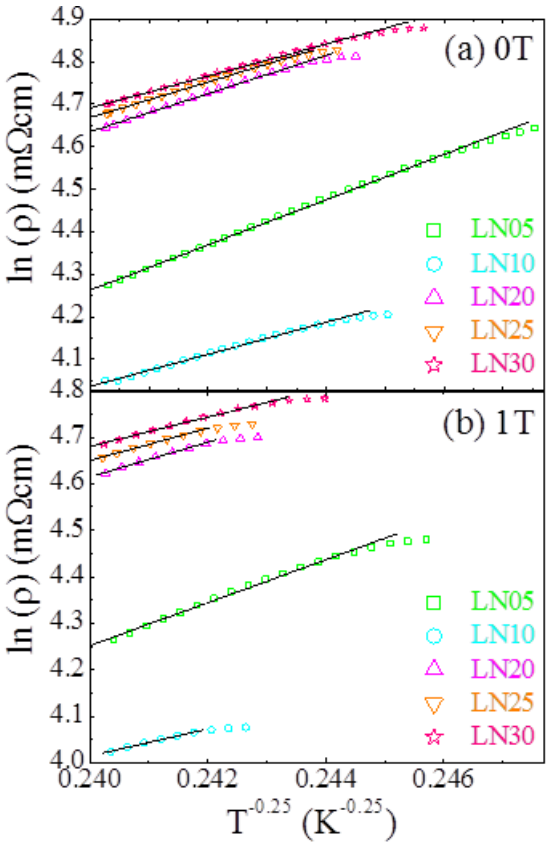

Fig. 4. Plots of fitting of resistivity data to ln ρ vs. $T^{-0.25}$ in semiconducting region under (a) 0T and (c) 1T applied magnetic fields for $La_{1-x}Na_xMnO_3$ (LNMO; x = 0.05, 0.10, 0.15, 0.20, 0.25 and 0.30) manganites

Fig. 4 shows the linear fits of resistivity data using Mott type VRH model for all the LNMO manganites (except LN15) under (a) 0T and (b) 1T applied magnetic fields. It is confirmed from the good agreement between the linear fits and resistivity (ln ρ) data that in the semiconducting region for all the LNMO samples, charge transport is governed by the VRH mechanism. Mott type VRH model having the form: $\rho=\rho_0 \exp(T_O/T)^{1/4}$, T_O is the carrier localization length which is directly related with an activation energy (E_a) by the formula: $E_a = T_O \times K_B$. Values of activation energy (E_a) under 0 and 1T applied magnetic fields for LNMO manganites are listed in **Table 2**. It is clearly seen from **Table 2** that with increase in Na–content (x) from 5% to 10%, E_a decreases which can be due to the increased charge carrier density (i.e. number of Mn^{4+} ions) resulting in the improved ZDE mechanism and hence conduction becomes easier in LN10 as compared to LN05 and hence E_a decreases. For Na–content (x) > 0.15, there exists a strong competition between the transport favorable: ZDE mechanism and tolerance factor, and transport degrading: size variance factor and super

exchange mechanism between two nearest Mn^{4+} ions via O^{2-} ion in the magnetic lattice. In addition, JT distortion becomes prominent over the semiconducting region, well above T_P for all the mixed valent perovskite manganites. As a result of complex competition between all the above transport related mechanisms, distortions and processes, E_a gets enhanced from Na–content (x) = 0.10 to 0.20 and then starts to decrease with further increase in Na–content (x).

Table 2. Values of activation energy (E_a) under 0 and 1T applied magnetic fields derived using VRH model fits to semiconducting region **(Fig. 4)** and power exponent (n) under 0, 1, 5 and 8T applied magnetic fields obtained using ZDE mechanism fits to metallic region **(Fig. 5)** for $La_{1-x}Na_xMnO_3$ (LNMO; x = 0.05, 0.10, 0.15, 0.20, 0.25 and 0.30) manganites

Sample	E_a (meV) (0T)	E_a (meV) (1T)	n (0T)	n (1T)	n (5T)	n (8T)
LN05	59.26	33.62	6.47	6.45	5.97	5.63
LN10	14.83	05.41	3.98	3.63	3.22	2.57
LN15	--	--	3.49	3.32	2.15	2.01
LN20	29.84	14.14	6.39	6.29	6.23	6.05
LN25	22.95	10.40	6.23	6.16	6.14	6.01
LN30	14.50	07.43	6.21	4.86	4.66	4.31

To understand the charge transport mechanism in metallic region well below T_P, in the temperature range: 80 – 200K under different applied magnetic fields, two different mechanisms have been used to fit theoretically the experimental resistivity data, namely, (i) small polaron conduction mechanism **[15]** and (ii) ZDE polynomial mechanism **[15, 25]** (not shown here). It was found that ZDE can properly explain the charge transport and charge carrier movement in the metallic region under all the applied magnetic fields for all the LNMO samples understudy. **Fig. 5** shows the resistivity fits using ZDE polynomial law (formula: $\rho_0 + \rho_2 T^2 + \rho_n T^n$; where ρ_0 – first term is resistivity contribution at 80K, $\rho_2 T^2$ is the resistivity contribution from electron – electron scattering, last term is contributing the resistivity due to electron – phonon and electron – magnon scattering processes and n is the power exponent) in the temperature range: 80 – 200K under (a) 0T, (b) 1T, (c) 5T and (d) 8T applied magnetic fields for all the LNMO samples. Factor of goodness of fits (χ^2) is found to be less than 10^{-11} suggests that theoretical expression is fitted well with the experimental resistivity data throughout the temperature range: 80 – 200K for all the applied magnetic fields and all the LNMO samples. Power exponent n = 2.5 and 3 refer to one magnon scattering mechanism, n = 4.5 and 7.5 refer to two magnon scattering process and n = 5.5 and 6.5 refer to intermediate scattering processes between the charge carrier electrons and magnetic lattice vibrations **[15, 25, 31]**. For the present study **Table 2**, n is found to decrease with increase in applied magnetic field for LNMO samples understudy which can be ascribed to the field induced suppression in the spin fluctuations in the Mn–O magnetic lattice. For LN05 sample, n varies between 6.5 and 5.5 suggesting a strong intermediate spin fluctuation and scattering processes. Upon increase in Na–content (x) from 0.05 to 0.10, n varies between 4 and 2.5 suggesting two and higher order magnon scattering effect under zero and low applied fields which becomes one magnon scattering under higher applied magnetic fields. Further increase in Na–content (x) from 0.10 to 0.15, LN15 possesses n in between 3.5 and 2 which suggests further suppressed spin fluctuation processes with increase in Na–content (x). Under high applied field of 8T, LN15 shows absence of electron – magnon scattering and only shows electron – electron scattering effect (n ~ 2). This can be correlated with the higher T_P amongst all the presently studied LNMO samples and lowest resistivity values, throughout the temperature range studied. It is clearly noticed from **Table 2** that with further increase in Na–content (x) from 0.15 to 0.30, all the samples possess higher order spin fluctuations (n is in between 4 and 6.5) which slightly decrease with increase in Na–content (x) from 0.20 to 0.30. This can be due to a strong competition between transport favoring and transport degrading mechanisms and processes.

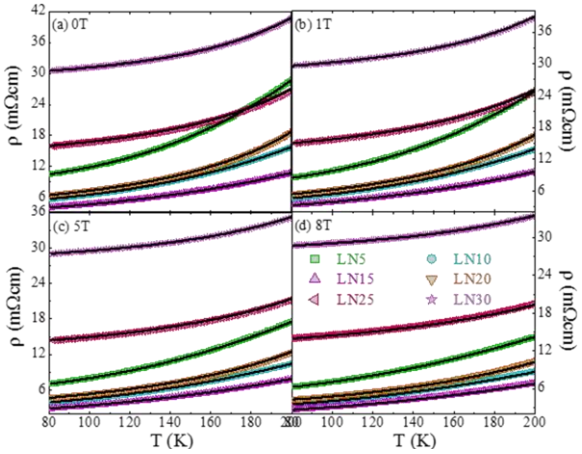

Fig. 5 Resistivity data of $La_{1-x}Na_xMnO_3$ (LNMO; x = 0.05, 0.10, 0.15, 0.20, 0.25 and 0.30) manganites carried out under (a) 0T, (b) 5T and (c) 8T fields fitted with ZDE polynomial law for the similar temperature range: 80 – 200K

In mixed valent manganites, at low temperature, charge carries (i.e. electrons) are localized due to existence of intrinsic efficient disorder. Below certain temperature (T_m), resistivity starts to increase with decrease in temperature, so called, resistivity minima behavior at low temperature. Various possible reasons for the understanding of this minima behavior can be employed such as grain boundary effect, phase separation, kondo effect and electron–electron scattering **[4, 32, 33]**. Similar resistivity minima behavior can be observed at low temperature for presently studied LNMO manganites (insets of **Fig. 2**). Phase separation scenario is effectively valid for nanoscale regime while kondo effect can also be ignored because it is only valid when magnetic lattice consists of non–magnetic impurities. The electron–electron scattering is one of an effective process which creates scattering for charge carriers and hence

is the source of resistivity in presently studied manganites. Since, samples are polycrystalline in nature possess granular microstructural behavior having different crystallographic orientations. Grain boundaries are disordered in nature hence act as scattering centers for charge carriers and block the electrons while passing across boundaries. In this context, reported electrostatic blockade model can be employed to understand the resistivity minima behavior in the presently studied LNMO manganites **[33]**.

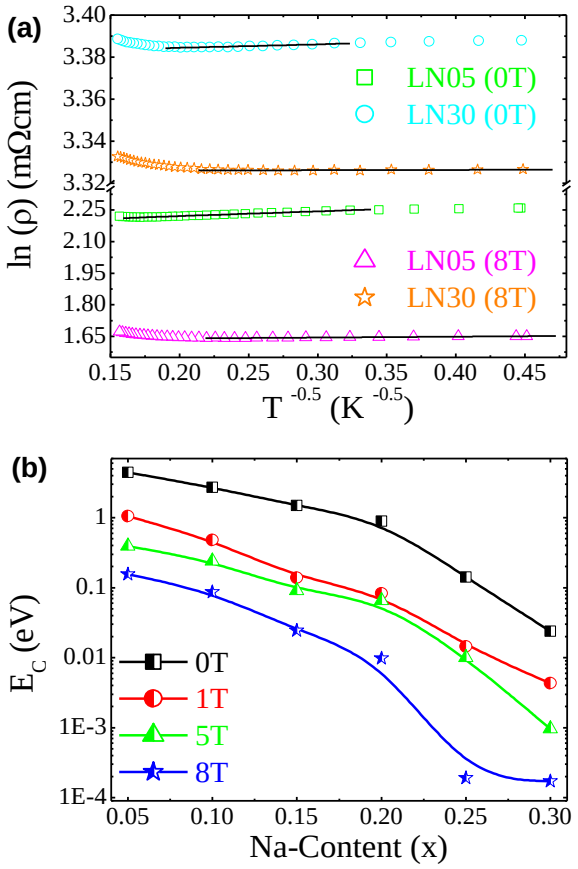

Fig. 6 (a) Typical dependence of ln (ρ) on $T^{-0.5}$ (0 – 40K) under zero and 8T applied magnetic fields for LN05 and LN30 manganite samples and (b) Na–content (x) dependence of electrostatic blockade energy (E_C) under different applied magnetic fields for $La_{1-x}Na_xMnO_3$ (LNMO; x = 0.05, 0.10, 0.15, 0.20, 0.25 and 0.30) manganites

Fig. 6 (a) shows the typical plots of log (ρ / ρ_{300}) vs. $T^{-0.5}$ (temperature range: 0 – 40K) for LN05 and LN30 samples under 0 and 8T applied magnetic fields. Plots have been fitted using straight line fits for verifying the validity of electrostatic blockade model having the form: ρ (T) = exp $(A/T)^{0.5}$ **[33]**. Parameter A is directly proportional to the electrostatic blockade energy (E_C) **[34, 35]**. **Fig. 6 (b)** shows the variation in electrostatic blockade energy (E_C) (in eV) with Na–content (x) under different applied magnetic fields for all the LNMO samples understudy. With increase in Na–content (x), E_C decreases which can be due to an increase in tolerance factor and hence improved transport favoring aspects (which dominate) in the presently studied mixed valent manganites. Upon increase in applied magnetic field, E_C decreases throughout the Na–content (x) range studied. This can be attributed to the magnetic field induced improved spin polarization and reduced Mn–O–Mn magnetic disorder at the grain boundaries, for all the LNMO manganites. Also, magnetic field provides a magnetic energy excess available with the charge carriers and hence easily passing through the grain boundaries across the lattice resulting in the suppression in electrostatic blocking energy.

Conclusion

In conclusion, effect of Na–content (x) in $La_{1-x}Na_xMnO_3$ (LNMO; x = 0.00, 0.05, 0.10, 0.15, 0.20, 0.25 and 0.30) mixed valent manganites has been studied for their structural and transport properties. The samples were grown using conventional ceramic method and structural properties of the samples were investigated by performing X-ray diffraction (XRD) measurement and Rietveld refinements for the XRD raw data. Rietveld refinements reveal the single phasic nature of all the compounds, having R–3C space group without any detectable impurity within the measurement range. Effect of larger monovalent Na^+ ion (1.24Å) substituted at smaller trivalent La^{3+} ionic site (1.216Å) on the structural properties has been discussed. Variation in peak resistivity (ρ_P) and metal to insulator transition temperature (T_P) with Na–content (x) has been understood on the basis of an effective competition between the transport favoring tolerance factor and zener double exchange (ZDE) mechanism and transport degrading size variance and Jahn–Teller (JT) effect for the presently studied LNMO manganite system. Nature of charge transport for insulating region exhibited by LNMO samples (except x = 0.15) has been understood on the basis of Mott type variable range hopping (VRH) mechanism and effect of Na–content (x) and applied magnetic field on the activation energy has been explored. Similarly, charge transport mechanism for the metallic region of all the LNMO samples has been discussed in the context of ZDE polynomial law and spin fluctuations in magnetic lattice and applied magnetic field induced modifications in the magnon scattering with charge carriers. Low temperature resistivity minima have been addressed by using electrostatic blockade model and variation in obtained electrostatic blocking energy (E_C) with Na–content (x) and applied magnetic field has been discussed in detail.

Acknowledgements

Author ZJ is thankful to UGC, New Delhi for financial support in the form of UGC (BSR) Meritorious Fellowship [File No.: F.25-1/2013-14(BSR)/7-156/2007(BSR)]. Author KNR is thankful to UGC, New Delhi for financial support in the form of UGC (BSR) Meritorious Fellowship [File No.: F.25-1/2014-15(BSR)/7-156/2007(BSR)]. Author KG is thankful to Inter University Accelerator Centre, New Delhi for financial assistance in the form of junior research fellowship [File No.: BTR 57309]. SK is thankful to UGC, New Delhi for financial support in the form of minor research project [File No.: 47–389/12(ERO)].

References

1. Dagotto, E.; Nanscale phase separation and colossal magnetoresistance: The physics of manganites and related compounds; Springer: USA, **2013**.
2. Kuberkar, D. G.; Doshi, R. R.; Solanki, P. S.; Khachar, Uma; Vagadia, Megha; Ravalia Ashish; Ganesan, V; *Appl. Sur. Sci.*, **2012**, *258*, 9041.
3. Ravalia, Ashish; Vagadia, Megha; Trivedi, Priyanka; Keshvani, M. J.; Khachar, Uma; Savalia, B. T.; Solanki, P. S.; Asokan, K.; Kuberkar, D. G; *Adv. Mater. Res.*, **2013**, *665*, 63.
4. Solanki, P. S.; Doshi, R. R.; Thaker, C. M.; Pandya, Swati; Ganesan V.; Kuberkar, D. G; *J. Nanosci. Nanotechnol*., **2009**, *9*, 5681.
5. Solanki, P. S.; Doshi, R. R.; Khachar, U. D.; Vagadia, M. V.; Ravalia, A. B.; Kuberkar D. G.; Shah, N. A; *J. Mater. Res.*, **2010**, *25*, 1799.
6. Solanki, P. S.; Doshi, R. R.; Khachar, U. D.; Choudhary R. J.; Kuberkar, D. G; *Mater. Res. Bull*., **2011**, *46*, 1118.
7. Solanki, P. S.; Doshi, R. R.; Khachar U. D.; Kuberkar, D. G.; *Phys. B*, **2011**, *406*, 1466.
8. Vachhani, P. S.; Solanki, P. S.; Doshi, R. R.; Shah, N. A.; Rayaprol, S.; Kuberkar, D. G; *Phys. B*, **2011**, *406*, 2270.
9. Kataria, Bharat; Solanki, P. S.; Khachar, Uma; Vagadia, Megha; Ravalia, Ashish; Keshvani, M. J.; Trivedi, Priyanka; Venkateshwarlu, D.; Ganesan, V.; Asokan, K.; Shah N. A.; Kuberkar, D. G.; *Rad. Phys. Chem*., **2013**, *85*, 173.
10. Rathod, J. S.; Khachar, Uma; Doshi, R. R.; Solanki, P. S.; Kuberkar, D. G.; *Int. J. Mod. Phys. B*, **2012**, *26*, 1250136.
11. Doshi, R. R.; Solanki, P. S.; Krishna, P. S. R.; Das A.; Kuberkar, D. G.; *J. Magn. Magn. Mater*., **2009**, *321*, 3285.
12. Krichene, A.; Bourouina, M.; Venkateshwarlu, D.; Solanki, P. S.; Rayaprol, S.; Ganesan, V.; Boujelben W.; Kuberkar, D. G.; *J. Magn. Magn. Mater*., **2016**, *408*, 116.
13. Solanki, P. S.; Khachar, Uma; Vagadia, Megha; Ravalia, Ashish; Katba Savan; Kuberkar, D. G.; *J. Appl. Phys*., **2015**, *117*, 145306.
14. Khachar, Uma; Solanki, P. S.; Choudhary. R. J.; Phase, D. M.; Ganesan V.; Kuberkar, D. G.; *Solid State Commun*., **2012**, *152*, 34.
15. Solanki, P. S.; Doshi, R. R.; Ravalia, Ashish; Keshvani, M. J.; Pandya, Swati; Ganesan, V.; Shah N. A.; Kuberkar, D. G.; *Phys. B*, **2015**, *465*, 71.
16. Krichene, A.; Solanki, P. S.; Rayaprol, S.; Ganesan, V.; Boujelben W.; Kuberkar, D. G.; *Ceram. Int*., **2015**, *41*, 2637.
17. Thaljaoui, R.; Pekala, K.; Pekala, M.; Boujelben, W.; Szydlowska, J.; Fagnard, J. F.; Vanderbemden, P.; Cheikhrouhou, A.; *J. Alloys Compd.*, **2013**, *580*, 117.
18. Thaljaoui, R.; Boujelben, W.; Pekala, M.; Pekala, K.; Fagnard, J. F.; Vanderbemden, P.; Donten, M.; Cheikhrouhou, A.; *J. Magn. Magn. Mater*., **2014**, *352*, 6.
19. Gadani, Keval; Dhruv, Davit; Joshi, Zalak; Boricha, Hetal; Vaghela, Eesh; Pandya, D. D.; Shah, N. A.; Solanki, P. S.; *AIP Conf. Proc*., **2016**, *1728*, 020516.
20. Boricha, Hetal; Dhruv, Davit; Joshi, Zalak; Alpa, Zankat; Pandya, D. D.; Joshi, A. D.; Solanki, P. S.; Shah, N. A.; *AIP Conf. Proc*., **2016**, *1728*, 020523.
21. Ho, T. A.; Dang, N. T.; Phan, T. L.; Yang, D. S.; Lee, B. W.; Yu, S. C.; *J. Alloys Compd.*, **2015**, *676*, 305.
22. Ehi–Eromosele C. O.; Ita, B. I.; Ajanaku, K. O.; Edobor–Osoh, A.; Aladesuyi, O.; Adalikwu, S. A.; Ehi–Eromosele, F. E.; *Bull. Mater. Sci.*, **2015**, *38*, 1749.
23. Arunachalam, M.; Thamilmaran, P.; Sankarrajan, S.; Sakthipandi, K.; *Cogent Phys.*, **2015**, *2*, 1067344.
24. Rodriguez Carvajel, J.; FULLPROF version 3.0 Laboratorie Leon Brillion, *CEACNRS*, **1995**.
25. Rathod, J. S.; Keshvani, M. J.; Solanki, P. S.; Pandya, D. D.; Kataria, Bharat; Shah N. A.; Kuberkar, D. G.; *Phys. B*, **2015**, *478*, 1.
26. Synder, G.; Hiskes, R.; Dicarolis, S.; Beasley M.; Geballe, T.; *Phys. Rev. B*, **1996**, *53*, 14434.
27. Ziese M.; Srinitiwarawong, C.; *Phys. Rev. B*, **1998**, *58*, 11519.
28. Efros A. L.; Shklovskii, B. L.; *J. Phys. C*, **1975**, *8*, L49.
29. Coey, J. M. D.; Viret, M.; Ranno L.; Ounadjela, K.; *Phys. Rev. Lett*., **1995**, *75*, 3910.
30. Viret, M.; Ranno L.; Coey, J. M. D.; *J. Appl. Phys*., **1997**, *81*, 4964.
31. Rana, D. S.; Thaker, C. M.; Mavani, K. R.; Kuberkar, D. G.; Kundaliya D. C.; Malik, S. K.; *J. Appl. Phys*., **2004**, *95*, 4934.
32. Rana, D. S.; Markna, J. H.; Parmar, R. N.; Kuberkar, D. G.; Raychaudhuri, P.; John J.; Malik, S. K.; *Phys. Rev*.B, **2005**, *71*, 212404. and references therein.
33. Lopez–Quintela, M. A.; Hueso, L. E.; Rivas J.; Rivadulla, F.; *Nanotechnology*, **2003**, *14*, 212.
34. Sheng, P.; Abeles B.; Arie, Y.; *Phys. Rev. Lett*., **1973**, *31*, 44.
35. Balcells, L; Martinez, B.; Sandiumenge F.; Fontcuberta, J.; *J. Phys.: Condens. Matter*, **2000**, *12*, 3013.